Structural Characterization of Gas Tungsten Arc Welded Stainless Steel at High Heat Input

*[1]Bolarinwa J. Kutelu, [2]Akinlabi Oyetunji, [2]Daniel T. Oloruntoba, [3]Raymond T. Oluyori
[1]Department of Mineral and Petroleum Resources Engineering Technology, The Federal Polytechnic, Ado-Ekiti, Ekiti State, Nigeria
[2]Department of Metallurgical and Materials Engineering, The Federal University of Technology, Akure, Ondo State, Nigeria.
[3]Department of Metallurgical and Materials Engineering, Kogi State Polytechnic, Lokoja, Kogi State, Nigeria
rinwa2006@yahoo.com | aoyetunji@futa.edu.ng | dtoloruntoba@futa.edu.ng | rtoluyori@gmail.com

Received: 05-AUG-2024; Reviewed: 28-AUG-2024; Accepted: 09-SEPT-2024
https://dx.doi.org/10.4314/fuoyejet.v9i3.20

ORIGINAL RESEARCH

Abstract- Performance integrity of weldment differs considerably from the base metal due to microstructural changes, resulting from welding heat input effect. In this study, effects of high gas tungsten arc welding heat inputs on microstructure of 304L austenitic stainless steel (ASS) weldments were investigated. The weldments were produced based on ASTM A778/778M at GTAW speed, current and voltage of 1.7 mm/s, 200 A and 40 V respectively. After which, they were characterised, using X-ray diffraction (XRD) and optical microscopy. The experimental samples, both control and weldments were prepared for the XRD and microstructural analysis following ASTM E 975-03 and ASTM E3 – 11 respectively. Results showed that control sample and weldments were characterized by varying amounts of major and minor compounds. Crystal structure of the control sample is comprised of a mixture of face centred cubic (FCC) and body centred cubic (BCC) with major peak (111). While those of the 1.7 mm/s, 200 A and 40 V produced weldments were comprised majorly of FCC with major peak (511), BCC with major peak (211) and BCC with major peak (110) respectively. Microstructure of the control sample is homogenous, comprising of equiaxed – grained austenite (γ) matrix with precipitates of varying sizes (dark spots), which are distributed non-uniformly within the γ matrix and small amounts of δ-ferrite (dark lines) along the γ matrix grain boundaries. While microstructures of the weldments are heterogeneous, comprising of austenite (γ) matrix and ferrite (α) grains, which are dispersed within the γ matrix. Generally, grains of the fusion zones (FZs) microstructures are fine relative the heat affected zones (HAZs) microstructures. The FZs and HAZs microstructures are characterised by precipitates, δ-ferrite, inclusions and dendrites of varied number and size.

Keywords: austenite (γ) matrix, equiaxed – grained, ferrite (α) grains, fusion zone (FZ), heat affected zone (HAZ), microstructures, weldments.

1 INTRODUCTION

304L austenitic stainless steel (ASS) is known for good combination of excellent corrosion resistance, good ductility and good weldability (Amer *et al.*, 2015; Hussain, 2010; Kožuh *et al.*, 2009). It has been successfully welded with shielded metal arc welding (SAW), submerged arc welding (SMAW), plasma arc welding (PAW) and gas tungsten arc welding (GTAW) techniques (Oyetunji *et al.*, 2013). Hence, its wide use as fabrication material for various industrial facilities, including oil and petrochemical fields, chemical plants, biomedical implants and food industries.

However, during welding, microstructure, surface texture and composition of the weld joint is influence by the welding heat inputs and, in consequence, mechanical and corrosion properties of the weld joint differ considerable from the base plate (Abioye, 2017; Apurv and Vijaykumar, 2014; Devakumar and Jabaraj, 2014; Ramesh and Chauhan, 2014; Kožuh *et al.*,2009). Therefore, adequate understanding of changes, occurring at the weld joint is necessary for making useful decision on the choice of welding parameters for production of the weldment either on industrial or domestic scale.

Corresponding Author: rinwa2006@yahoo.com

Section D- MATERIALS AND METARLLUGY/CHEMICAL SCIENCES & RELATED SCIENCES
Can be cited as:
Kutelu B. J.,Oyetunji A., Oloruntoba D. T. and Oluyori R. T. (2024). Structural Characterization of Gas Tungsten Arc Welded Stainless Steel at High Heat Input (FUOYE**JET), 9(3), 496-502.**

https://dx.doi.org/10.4314/fuoyejet.v9i3.20

Consequently, in this study, high heat input inducing parameters were considered, because influence of heat input on either mechanical or corrosion performance of the weld joint is more severe at high heat input.

2 METHODOLOGY

2.1 CHEMICAL COMPOSITION

Chemical compositions of the as-received 304L ASS plate and filler rod employed for the production of the weldments were obtained by optical emission spectrometry (AR 4 30 metal analyser), and the results are presented in Tables 1 and 2 respectively

Table 1. Chemical composition of the experimental as-received 304L ASS plate

Element	Wt. %	Element	Wt. %	Element	Wt. %
C	0.026	Cr	18.325	Cl	0.002
Si	0.511	Ni	8.469	Mo	0.069
Mn	1.311	Cu	0.135	V	0.083
S	<0.001	Nb	0.009	Ti	0.036
P	0.013	Al	0.018	Fe	75.916

Table 2. Chemical composition of the filler metal

Element	Wt. %
C	<0.03
Mn	1.650
Si	0.65
P	0.03
S	0.03
Cr	19.5-22.0
Ni	9.0-11.0

2.2 Sample Preparation

Samples of dimensions 120 mm × 20 mm × 8 mm were cut from the as-received 304L ASS plate, using simple handsaw, and they were cleaned with acetone to remove lubricant and surface contamination. The samples were machined to butt – joint to make a single – V groove of 60° with root gap of 2.5 mm, this configuration was maintained to ensure good root penetration (Janunkar *et al.*, 2017) The welding parameters were fixed at 1.7 mm/s, 200A and 40V, corresponding to high heat input. Multipass welding was conducted on the samples, using Clark TIG welding machine and 2.5 mm diameter filler electrode. The values of current and voltage were read directly from the GTAW machine, while values of speed were obtained by calculation using the expression in Eqn. 1 [24]. The weldments were visually inspected for any weld defects and/or geometrical non-conformity. Table 3 summarises the procedure for the weldment production and Table 4 shows the quantities of heat input at the varied GTAW parameters, and Fig. 1 and Fig. 2 are samples of the butt-joint with single – V configuration and the produced weldment.

$$S = \frac{L}{T} \quad (1)$$

Where S is welding speed (mm/s), L is length (mm) and T is time (s). The time taken to produce each weldment was determined using a stop watch.

Table 3. Summary of the procedure for weldments production

S/No	Welding parameters		
1.	Speed (mm/s	Current (A)	Voltage (V)
2.	1.7 Current (A)	160 Speed (mm/s	30 Voltage (V)
3.	200 Voltage (V)	4.6 Current (A)	30 Speed (mm/s)
	40	160	30

Table 4. Quantity of heat input at the varied GTAW parameters

S/No.	Welding parameters			Heat input (J/mm)
1.	Speed (mm/s)	Current (A)	Voltage (V)	
2.	1.7 Current (A)	160 Speed (mm/s)	30 Voltage (V)	1694.5
3.	200 Voltage (V)	4.6 Current (A)	30 Speed (mm/s)	782.61
	40	160	4.6	834.78

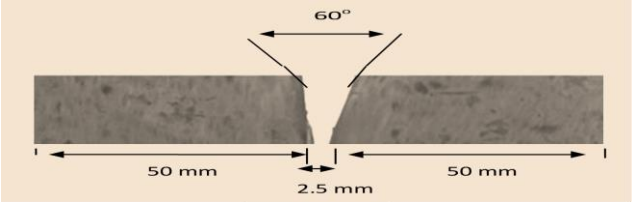

Fig. 1. Butt joint sample with single-V configuration

Fig. 2. Sample of the GTAW 304L ASS weldment

2.3 X-Ray Diffraction (XRD) Measurement

The XRD samples were prepared in accordance with ASTM E 975-03. Phase constituents of the samples were obtained at room temperature (25°C), using Philips X'Pert diffractometer under Cu-Kα radiation with measuring accuracy of 5%. Data were collected over the 2θ range of 10o to 80o with a step size of 0.05° and an exposition time of 2 s per step, X'Pert High Score plus software was used to analyse the data.

2.4 Optical Microscopy

The metallographic samples were prepared based ASTM E3-11. Conventional metallographic grinding and polishing techniques were used to achieved the desired surface finish. The samples were etched in solution of 50 ml HCl + 50 ml HNO_3 + 50 ml water for two minutes. FZ and HAZ microstructures were viewed and captured, using optical metallurgical microscope (OMM) (Olympus GX51) with camera attached.

2http://dx.doi.org/10.46792/fuoyejet.v9i3.20 engineering.fuoye.edu.ng/journal

3 Results and Discussion

3.1 X-Ray Diffractometer (XRD) Analysis

Fig. 3 and Fig. 4 are XRD diffractogram and stick pattern of the control sample respectively, and Table 5 and Table 6 are the peak list and identified pattern list respectively. From the results, The major peak, corresponding to X, Y and Z planes is (111), and minor peaks, corresponding to X, Y and Z planes are (200), (220), (311) and (222). Compounds of the major peak are Co3 Fe_7, Fe $_{0.64}$ and $Ni_{0.36}$, those of the minor peaks are $Cr_{1.36}$ Fe $_{0.52,}$ Cr and Cr Si (Table 6). The sample is comprised of a mixture of face centred cubic (FCC), corresponding to austenite (γ-Fe) phase, and body centred cubic (BCC), corresponds to ferrite (α-Fe) phase. The control is therefore not fully austenitic, but predominantly austenitic (Kožuh *et al.*, 2009; Honeycombe and Bhadeshia, 1995). And its chromium content of 18.325% (refer to Table 1) was indicative of its good to excellent corrosion resistance (Kožuh *et al.*, 2013). The x-ray diffractogram and stick pattern of weldment produced at the speed of 1.7 mm/s are shown Figs. 5 and 6 respectively, and the identified peak list and pattern list are depicted in Table 7 and Table 8 respectively.

From the results, the major peak, corresponding to X, Y and Z planes is (511), and the other identified minor peaks, corresponding to X, Y and Z planes are (111), (200), (220), (311), (222), (400), (331), (420), (422), (440), (531) and (600). Compounds of the major peak are C, Ni_3 Zn $C0_{.7}$, Cr $_{1.36}$ Fe $_{0.52,}$ and those of the minor peak are Fe Ni. Mn_6 Ni_{16} P_7, Si O_2, Mn_3 Co_7, Fe_7 S_8, Ni O and Cr.

The crystal structure of the weldment is FCC, corresponding to (γ-Fe) phase. Hence, it is fully austenitic (Kožuh *et al.*, 2009). Fig. 7 and Fig. 8 are the X-ray diffractogram and stick pattern of weldment produced at the current of 200A respectively, and the corresponding identified peaks list and pattern list are shown in Table 9 and Table 10 respectively, the major peak, corresponding to X, Y and Z plane is (211). Other identified minor peaks lists, corresponding to X,Y and Z planes are (200), (211), (220), (310) and (222). Compounds of the major peaks are Fe-Cr and Cr, and those of the minor peaks are Ni_3 Zn $C0_{.7}$, Ni O, Fe Si, C, Fe_3 O_4, Ni and Mn Si. The crystal structure of the weldment is BCC, corresponding to α-Fe phase. Hence, the weldment is comprised majorly of ferrite (Kožuh *et al.*, 2009). X-ray diffractogram and stick pattern of weldment produced at the voltage of 40V are depicted in Fig. 9 and Fig. 10 respectively, and the identified peak list and pattern list are shown in Table 11 and Table 12 respectively. The major peak, corresponding to X,Y and Z is (110). Other minor peaks, corresponding to X,Y and Z planes are (200), (220), (222), (321) and (332). Compounds of the major peaks are Fe-Cr and Cr, and those of the minor peaks are $C_{0.14}$ $Fe_{1.86,}$ (Ni O)$_{.75}$ (Mn O)$_{.25}$, Cr. Crystal structure of the weldment is BCC, corresponding to α-Fe phase. Hence, the weldment is comprised majorly of ferrite (Kožuh *et al.*, 2009).

In general, increasing volume fraction of ferrite (i.e. α-Fe phase) of the weldments relative to the control sample may be attributed to high welding heat inputs, and hence slow cooling conditions of the solidification process, during which, sufficient time was provided for transformation of γ-Fe to α-Fe (Atapour *et al.*, 2015). The long peaks of the weldments relative to the control sample was due to grain coarseness that resulted from slow cooling condition of the solidification process. This is because the significant relationship that existed between grains refinement and peak shortening has been attributed to fast cooling conditions, accompanying solidification process (Fowless and Blake, 2008).

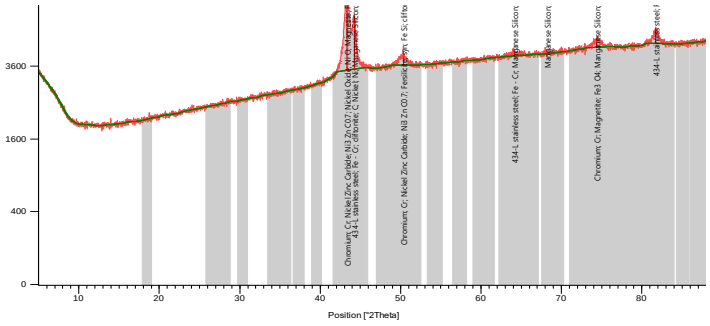

Fig. 3. XRD diffractogram of control sample

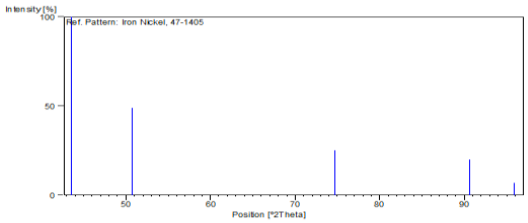

Fig. 4. Stick pattern of the control sample

Table 5. Identified peak list of control sample

S/N.	h	K	l	d(A)	I (%)
1	1	1	1	2.07400	100.0
2	2	0	0	1.79600	49.0
3	2	2	0	1.27000	25.0
4	3	1	1	1.08340	20.0
5	2	2	2	1.03730	7.0

2http://dx.doi.org/10.46792/fuoyejet.v9i3.20 engineering.fuoye.edu.ng/journal

Table 6. Identified patterns list of control sample

Score	Compound	Scale Factor	Chemical Formula
51	Cobalt Iron	0.015	$Co_3 Fe_7$
39	Iron Nickel	0.170	$Fe_{0.64} Ni_{0.36}$
26	Chromium Iron	0.019	$Cr_{1.36} Fe_{0.52}$
25	Chromium	0.012	Cr
25	Chromium Silicon	0.902	Cr Si

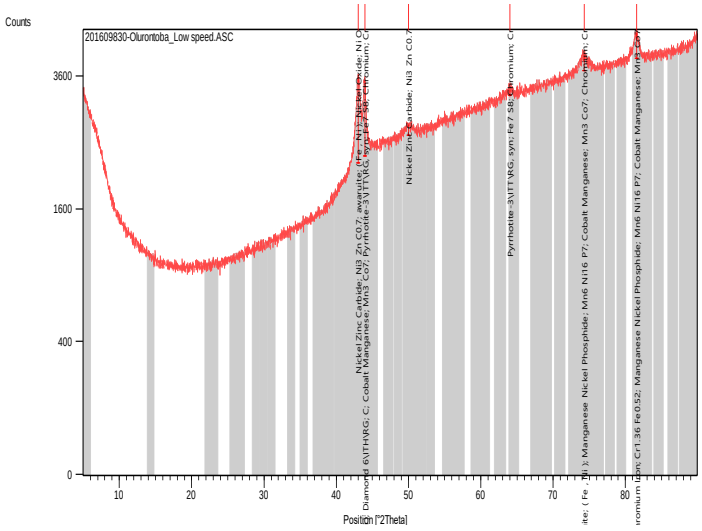

Fig. 5. XRD Spectrum of weldment speed 1.7mm/s

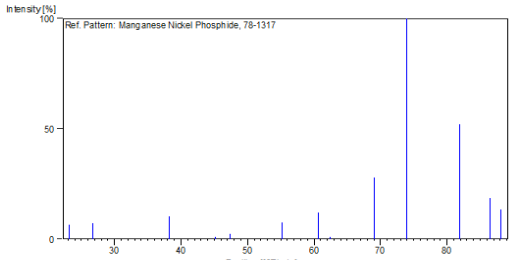

Fig. 6. XRD stick pattern of weldment at speed 1.7 mm/s

Table 7. Identified peak list of weldment at speed 1.7 mm/s

S/N	h	k	l	d[A]	I [%]
1	1	1	1	3.83880	6.4
2	2	0	0	3.32450	7.2
3	2	2	0	2.35078	10.2
4	3	1	1	2.00475	0.1
5	2	2	2	1.91940	2.3
6	4	0	0	1.66225	7.6
7	3	3	1	1.52539	12.0
8	4	2	0	1.48676	0.2
9	4	2	2	1.35722	27.8
10	5	1	1	1.27960	100.0
11	4	4	0	1.17539	52.0
12	5	3	1		18.6
13	6	0	0	1.10817	13.3

Table 8. Identified patterns list of weldment at speed of 1.7 mm/s

Score	Compound Name	Scale Factor	Chemical Formula
46	Diamond 3\ITC\RG	0.804	C
45	Nickel Zinc Carbide	0.546	$Ni_3 Zn C0.7$
38	Chromium Iron	0.113	$Cr_{1.36} Fe_{0.52}$
39	Awaruite	0.247	(Fe , Ni)
27	Manganese Nickel Phosphide	0.204	$Mn6 Ni_{16} P_7$
19	Silicon Oxide	2.107	$Si O_2$
21	Cobalt Manganese	0.362	$Mn_3 Co_7$
22	Pyrrhotite-3\ITT\RG, syn	0.391	$Fe_7 S_8$
18	Nickel Oxide	0.420	Ni O
22	Chromium	0.157	Cr

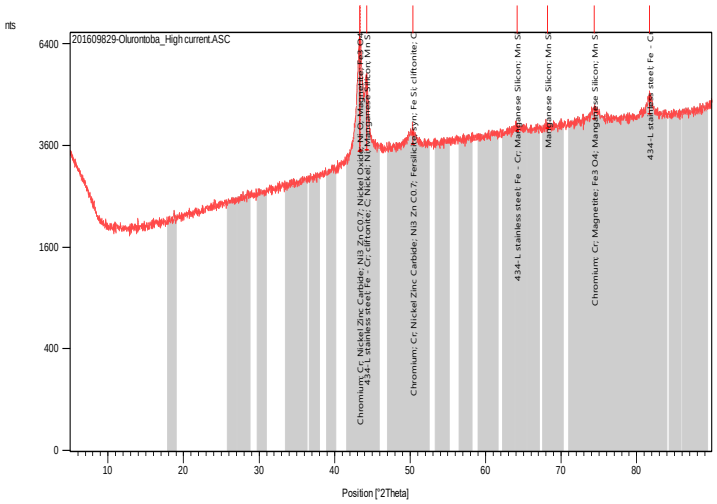

Fig. 7. XRD spectrum of the weldment at current of 200 A

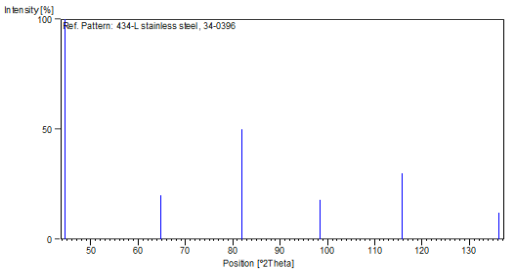

Fig. 8. Stick pattern of the weldment at current of 200 A

2http://dx.doi.org/10.46792/fuoyejet.v9i3.20 engineering.fuoye.edu.ng/journal

Table 9. Identified peak list of the weldment at current of 200 A

S/N	h	k	l	d [A]	I [%]
1	2	1	1	2.03500	100.0
2	2	0	0	1.43800	20.0
3	2	1	1	1.17430	50.0
4	2	2	0	1.01700	18.0
5	3	1	0	0.90950	30.0
6	2	2	2	0.83020	12.0

Table 10. Identified pattern list of the weldment at current of 200 A

Score	Compound Name	Scale Factor	Chemical Formula
56	304-L stainless steel	0.212	Fe – Cr
52	Chromium	0.614	Cr
29	Nickel Zinc Carbide	0.206	Ni_3 Zn $C0_{.7}$
21	Nickel Oxide	0.770	Ni O
18	Fersilicite, syn	0.100	Fe Si
9	Cliftonite	0.035	C
11	Magnetite	0.157	Fe_3 O_4
34	Nickel	0.162	Ni
18	Manganese Silicon	0.220	Mn Si

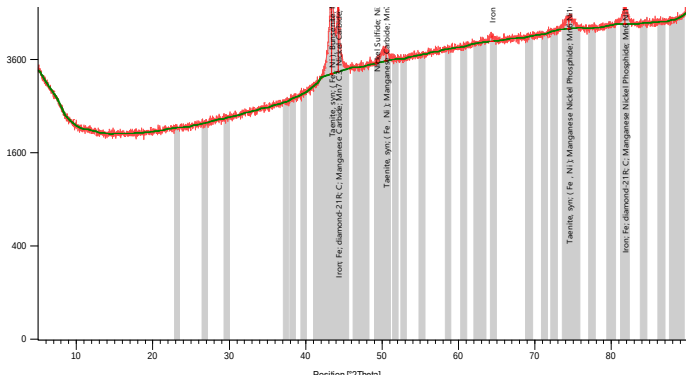

Fig. 9. XRD Spectrum of the weldment at voltage of 40 V

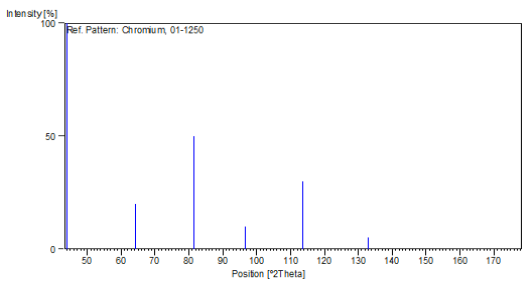

Fig. 10. Stick pattern of the weldment at voltage of 40 V

Table 11. Identified peak list of the weldment GTAW at current of 40V

S/N	h	k	l	d [A]	I [%]
1	1	1	0	2.05000	100.0
2	2	0	0	1.45000	20.0
3	2	2	0	1.03000	10.0
4	2	2	2	0.84000	5.0
5	3	2	1	0.77000	30.0
6	3	3	2	0.62000	2.0

Table 12. Identified pattern list of the weldment at GTAW current of 40V

Score	Compound Name	Scale Factor	Chemical Formula
57	Chromium	0.860	Cr
36	Martensite	0.549	$C0_{.14}$ $Fe_{1.86}$
25	Chromium	0.183	Cr
17	Nickel Manganese Oxide	0.416	(Ni O).75 (Mn O).25
24	Silicon Oxide	0.341	$Si O_2$
33	Chromium Silicon	0.699	Cr Si_2

3.2 Microstructural Analysis of the Samples

Plates 1(A-D) are microstructures of the control sample, and weldments at the speed, current and voltage of 1.7 mm/s, 200 A and 40V respectively. The control sample is characterized by austenite matrix of equiaxed – grains with small amount of δ – ferrite along the grain boundaries. In addition, non-uniformly distributed varying sizes of precipitates are visible within the austenite matrix. Microstructures of weldments, comprising FZs and HAZs are characterised by fine and coarse grains respectively. Similar to the control sample, the microstructures are characterised by a number of δ – ferrite and precipitations of varying sizes, and unlike the control sample, the weldments (FZs and HAZs) are comprised of inclusions and dendrites of different sizes. The small amount of δ – ferrite along the grain boundaries of the control sample may have been introduced intentionally to address problem of hot cracking that resulted from segregation of low melting point elements such as sulphur and phosphorus along the austenite grain boundaries (Lawrence et al., 2016; Kožuh et al., 2009), and

2http://dx.doi.org/10.46792/fuoyejet.v9i3.20 engineering.fuoye.edu.ng/journal

the precipitates may have resulted from thermal history of the sample (Amer et al., 2015; Kurt and Samur, 2013;Hussain, 2010; Kožuh et al., 2009). In general, weld cooling conditions are governed by heat, and hence microstructural heterogeneity and dendrites of different sizes, characterizing the weldment were expected, and they may have resulted from temperature gradient that was generated by the resulting welding heat input of the GTAW technique (Ghusoon et al., 2017; Pauli et al., 2016; Achebo, 2012), and chemical gradients that were due to the GTAW heat input may have contributed to the microstructural characteristics of the weldments (Lawrence et al., 2016; Tabish et al., 2014). The obvious inclusions within the FZs and HAZs of the weldments may be due to possible chemical reactions between dissolved metallic elements such as Fe, Mn, Al, Si and Cr and non- metallic elements such as S and C (Ramesh and Chauhan, 2014; Çalik, 2009). In addition, the inclusions may have resulted from oxidation at the weld pool surface, leading to the combination of some elements, including Mn, Si, Al with oxygen at high temperature to form a single phase oxide of MnO – SiO2–Al2O3 (Costa, 2018; Bhatti et al., 1984). In comparison, GTAW heat input at the welding speed of 1.7 mm/s is high relative to voltage of 40V and current of 200A correspondingly, as evident in the relative numbers of inclusion and dendrite, and number of peak and peak shortening (refer to Tables). Hence, structural characteristic features of the weldments were differently influenced at the GTAW speed, current and voltage.

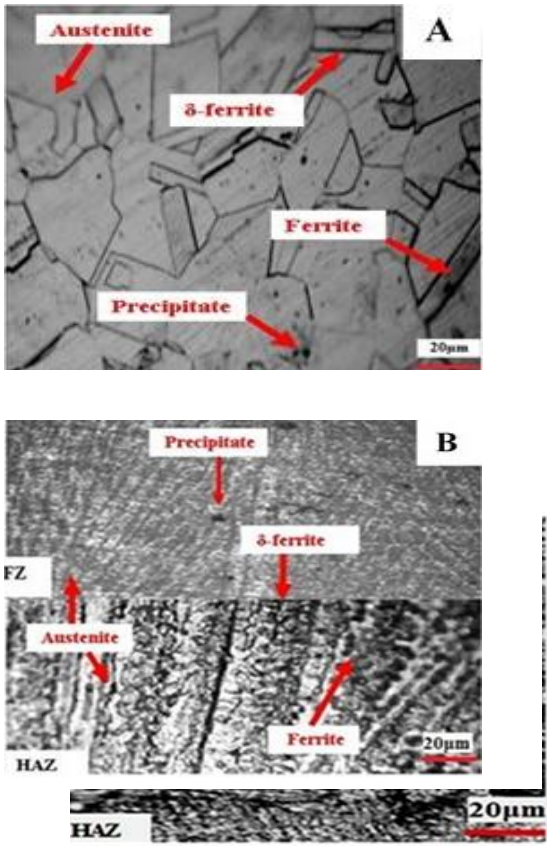

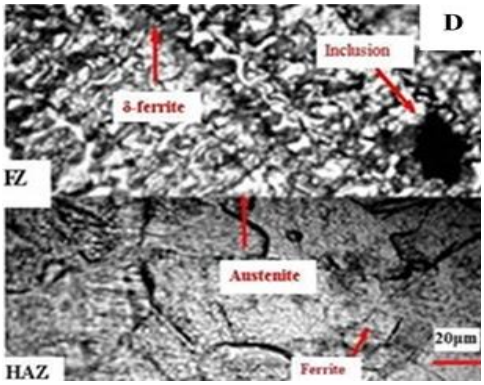

Plate 1 (A-D). Microstructures of the Control, weldments at the speed of 1.7 mm/s, 200 A and 40 V of current and voltage respectively at magnification 400xx

4 CONCLUSION

Based on the results of the investigations, the following conclusions were drawn:

1. The control sample and weldments are characterized by varying amounts of major and minor compounds.
2. Crystal structure of the control sample is comprised of a mixture of face centred cubic (FCC) and body centred cubic (BCC) with major peak (111). While those of the 1.7 mm/s, 200 A and 40 V produced weldments were comprised majorly of FCC with major peak (511), BCC with major peak (211) and BCC with major peak (110) respectively.
3. Microstructure of the control sample is homogenous, comprising of equiaxed – grained austenite (γ) matrix. Non-uniformly distributed precipitates of varying sizes (dark spots) and small amounts of δ-ferrite (dark lines) are found within the γ matrix and along the γ matrix grain boundaries respectively.
4. Microstructures of the weldments are heterogeneous, comprising of austenite (γ) matrix and ferrite (α) grains, which are dispersed within the γ matrix. Gains of the fusion zones (FZs) microstructures are fine relative to grains of the heat affected zones (HAZs) microstructures, and varied numbers and sizes of precipitates, δ-ferrite, inclusions and dendrites

2http://dx.doi.org/10.46792/fuoyejet.v9i3.20 engineering.fuoye.edu.ng/journal

are visible within the FZs and HAZs microstructures.

REFERENCES

Abioye, T. E. (2017). Effect of Heat input on the mechanical and corrosion properties of AISI 304 electric arc weldments, *British Journal of Applied Science and Technology*, 20, 1-10

Achebo, J. I. (2012). Influence of alloying elements on haz toughness of multilayer welded steel joints. *International Journal of Advances in Science and Technology*, 3 (4), 78 - 83.

Apurv, C. & Vijaykumar, S. J. (2014). Influence of heat input on mechanical properties and microstructure of austenitic 202 grade stainless steel Weldments, *WSEAS Transactions on Applied and Theoretical Mechanics*, 9, 222-228

Amer, S. M., Morsy, M. A., Hussein. M. .A.,Atlam, A. & Mosa E. S. (2015) Effect of welding parameters variation on the weldability of austenitic stainless steel 304L, *International Journal of Scientific and Engineering Research*, 6 (2)2, 589-595.

American Standard for Testing and Measurement (ASTM) E3 11(2011). Standard guide for preparation of metallographic specimens, ASTM International, West Conshohocken, www.astm.org.

Atapour, M., Dana, M. M. & Ashrafizadeh, F. (2015). A corrosion study of grain-refined 304l stainless steels produced by the martensitic process, *International Journal of ISSI*, 12 (2), 30-38

Bhatti, A. R., Saggese, M. E., Hawkins, D. N., Whiteman, J. A. & Golding, M. S. (1984) Analysis of inclusions in submerged arc welds in micro alloyed steels, *Welding Journal*, 63(7), 224-230.

Çalik, A. (2009) Effect of cooling rate on hardness and microstructure of AISI 1020, AISI 1040 and AISI 1060 steels, *Int. J. of Phys. Sci*, 4 (9), 514-518. 2009.

Costa, S. (2018) Non-metallic inclusions in steels – Origin and Control (Review)". *J. Mater Res Technol*, 283-299. 2018.

Devakumar, D. & Jabaraj, D. B. (2014) Research on gas tungsten arc welding of stainless steel-an overview, *International Journal of Scientific and Engineering Research*, 5 (1), 1612–1618.

Fowless, R. J. and Blake, S. E. (2008) Influence of heat input on austenitic stainless steel, *Weld Properties African Fusion*, 1 (2), 17 24.

Ghusoon, R. M., Mahadzir, I., Syarifah, N. A. & Hassan A. A. (2017). Effects of heat input on microstructure, corrosion and mechanical characteristics of welded austenitic and duplex stainless steels, A review, *Metals*, 7(39), 123-136.

Gigović-Gekić, A., Oruč, M. & Gojić, M. (2011). Determination of the content of delta ferrite in austenitic stainless steel nitronic 60, in proceedings of 15th international research/expert conference, prague, Czech Republic, 157-160.

Honeycombe, R.W.L. & Bhadeshia, H.K.D.H. (1995). Steel microstructure and properties, metals and materials series, Edward Arnold, Hodder-Heading, London, England, 65-71.

Hussain, A.K. (2010). Influence of welding speed on tensile strength of welded joint in TIG welding process, *International Journal of Applied Engineering Resources*, 518.

Janunkar, R. G., Allurkar, S. & Mahesh, P. (2017) .An influence on effecof welding speed on strength of welded joint using TIG welding process, *World Journal of Technology, Engineering and Research*, vol. 2, no1, pp. 337-342.

Kondapalli, S. P., Ch.Srinivasa, R. D. & Nageswara, R. (2011). Optimizing fusion zone grain size and ultimate tensile strength of pulsed current micro plasma arc welding welded SS304L sheets using hooke and jeeves algorithm, Proceedings of International Conference on Futuristic Trends in Materials and Energy Systems, V R Siddhartha Engineering College, Vijayawada, A.P., India, 112-119.

Kožuh, S M.. Goji´c, M., Vrsalovi´c, L. & Ivkovi´c, B. (2013). Corrosion failure and microstructure analysis of AISI 316 stainless steels for ship pipeline before and after welding, *Kovove Mater*,51,53-61

Kožuh, S., Goji´c. M. & Kosec. L. (2009), Mechanical properties and microstructure of austenitic stainless steel after welding and post-weld heat treatment, *Kovove Mater.* 47, 253–262.

Kurt, H.I. & Samur, R. (2013). Study on microstructure, tensile test and hardness 304 stainless steel jointed by TIG welding, *International Journal of Science and Technology*, 2 (2), 164-168.

Lawrence, O. O., Raheem, A. E. & Ikenna, C. E. (2016). Influence of delta ferrite on corrosion susceptibility, of AISI 304 austenitic stainless steel, *Materials Engineering Research Article*,9,120-128.

Oyetunji, O., Kutelu, B.J. & Akinola, A.S. (2013). Effects of welding speeds and power inputs on the hardness property of type 304L austenitic stainless steel heat-affected zone (HAZ), *Journal of Metallurgical Engineering (ME)*, 2 I, 124-129.

Pauli, L., Jani, R., Heikki, R. & Teemu, S. (2016). Characterization of local grain size variation of welded structural steel, *Weld World*, 60, 673–688.

Ramesh, k, N. & Chauhan, P.M. R (2014). Mechanical properties and microstructural investigations of TIG welded 40 mm and 60 mm thick SS 316L samples for fusion reactor vacuum vessel applications, *Fusion Engineering and Design*, 89, 3149–3158.

Tabish, T. A., Abbas, T., Farhan, M., Atiq, S. & Butt, T. Z. (2014). Effect of heat input on microstructure and mechanical properties of the TIG welded joints of AISI 304 stainless steel, *International Journal of Scientific and Engineering Research*, 5 , 1526 – 1532.

Thewlis, C. & Milner D. R. (1977). Inclusion formation in arc welding, *Welding Research Supplement*, 281-288.

2http://dx.doi.org/10.46792/fuoyejet.v9i3.20 engineering.fuoye.edu.ng/journal